

# Compressive sensing as a new paradigm for model building

Lance J. Nelson and Gus L. W. Hart

*Department of Physics and Astronomy, Brigham Young University, Provo, Utah 84602, USA*

Fei Zhou (周非) and Vidvuds Ozoliņš

*Department of Materials Science and Engineering,  
University of California, Los Angeles, California 90095, USA*

(Dated: March 8, 2022)

The widely-accepted intuition that the important properties of solids are determined by a few key variables underpins many methods in physics. Though this reductionist paradigm is applicable in many physical problems, its utility can be limited because the intuition for identifying the key variables often does not exist or is difficult to develop. Machine learning algorithms (genetic programming, neural networks, Bayesian methods, etc.) attempt to eliminate the a priori need for such intuition but often do so with increased computational burden and human time. A recently-developed technique in the field of signal processing, compressive sensing (CS), provides a simple, general, and efficient way of finding the key descriptive variables. CS is a new paradigm for model building—we show that its models are just as robust as those built by current state-of-the-art approaches, but can be constructed at a fraction of the computational cost and user effort.

## I. A NEW PARADIGM

Intuition suggests that important properties of materials are primarily determined by just a few key variables. Examples of such cases are numerous. For instance, the crystal structures of intermetallic compounds have been successfully classified into groups (so-called structure maps) according to the properties of the constituent atoms,<sup>1–4</sup> the seminal Miedema rules relate alloy formation energies to atomic charge densities and electronegativities,<sup>5</sup> and some magnets can be described using a Heisenberg model with only a few well-chosen interactions.

The difficulties with this “canonical approach” of finding a few descriptive variables is that the intuition for choosing them often does not exist or is difficult to develop, and there is no clear path to achieve systematic improvement. Machine learning algorithms (genetic programming, neural networks, Bayesian methods, etc.) attempt to overcome these challenges at the cost of increased algorithmic complexity.<sup>6–13</sup> We show that a recently developed technique in the field of signal processing, compressive sensing (CS)<sup>14</sup>, provides a simple, general, and efficient way of finding the key descriptive variables.<sup>15</sup> CS is a new paradigm for model building—its models are just as robust as those built by current state-of-the-art approaches, but can be constructed at a fraction of the computational cost and user effort.

## II. COMPRESSIVE SENSING: AN ILLUSTRATION

In a signal processing context, compressive sensing can recover so-called “sparse” signals *exactly* with far fewer samples than required for standard spectral techniques, such as the famous Fourier and Laplace transforms. When applied to the task of building physical

models, the power of compressive sensing is that a physical quantity can be predicted with high fidelity using a small number of experiments or calculations as training data.

Before demonstrating the power of compressive sensing for building materials models, we first demonstrate the concept itself with a simple time series. Consider a signal like that shown in Fig. 1(a) which has the functional form:

$$f(t) = \sum_{n=1}^N u_n e^{i2\pi n t}, \quad (1)$$

where most of the coefficients,  $u_n$ , are zero (i.e., the signal is sparse). The Fourier transform is mathematically equivalent to solving the matrix equation

$$\mathbb{A} \vec{u} = \vec{f}, \quad (2)$$

where the matrix  $\mathbb{A}$  is formed by the values of the Fourier basis functions at the sampling times  $t_m$ , i.e., it consists of rows of  $n$  terms of the form  $A_{mn} = e^{i2\pi n t_m}$ , and  $f_m \equiv f(t_m)$  is the sampled signal. The solution vector  $\vec{u}$  contains the relative amounts of the different Fourier components, as shown in Fig. 1(b). Capturing all relevant frequency components of the signal using Fourier transform techniques requires the signal to be sampled regularly and at a frequency at least as high as the Nyquist frequency (shown as red points in Fig. 1(a)), a severe restriction arising from the requirement that the linear system Eq. (2) should not be underdetermined.

However, when the signal is sparse, one should be able to recover the exact signal with a number of measurements that is proportional to the number of nonzero components, i.e., with far fewer samples than given by the Nyquist frequency. This is an underdetermined and therefore intractable problem using traditional spectral decomposition techniques. Conceptually, compressive sensing solves this problem by searching for a solution

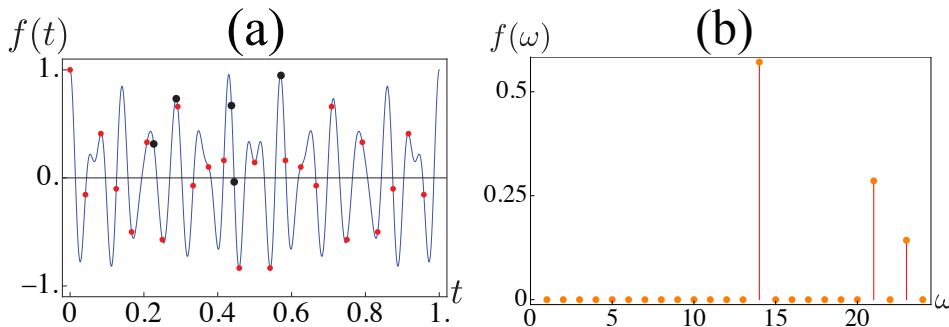


FIG. 1. (a) A sparse signal (blue line) like that of Eq. 1, uniform samples of the signal at the Nyquist frequency (red dots), and a few random samples (black circles). The signal is composed of only 3 non-zero frequencies. (b) Exact recovery of the frequency components of the signal using compressive sensing.

that reproduces the measured time signal *and* has the minimum number of non-zero Fourier components. Formally, this is done by reformulating the problem as a simple minimization of the  $\ell_1$  norm (see Method) of the solution, subject to the constraint given by Eq. (2) above:

$$\min_{\vec{u}} \{ \|\vec{u}\|_1 : \mathbf{A}\vec{u} = \vec{f} \}, \quad (3)$$

where  $\|\vec{u}\|_1 = \sum_i |u_i|$  is the  $\ell_1$ -norm. In other words, we seek to minimize the components of the vector  $\vec{u}$  subject to the condition that the measured signal is reproduced exactly; this constitutes the so-called basis pursuit problem. Note that the optimization of the common sum-of-squares ( $\ell_2$ ) norm usually does not lead to sparse solutions.<sup>14</sup>

The exact decomposition of an example function, shown in Fig. 1, was possible via compressive sensing with only 5 random samples of the signal, instead of the 24 equally-spaced samples needed for a discrete Fourier transform. Quite generally, a theorem proven by Candes, Romberg, and Tao<sup>16</sup> guarantees that, with an overwhelming probability, any sparse signal with  $S$  nonzero components can be recovered from a number of randomly chosen measurements  $M$  that is proportional to  $S \log N$ , where  $N$  is the total number of basis functions [see, e.g., Eq. (1)]. This very powerful result is the mathematical foundation of compressed sensing.

### III. COMPRESSIVE SENSING FOR MODEL BUILDING

Here, we show that  $\ell_1$ -based compressive sensing (CS) can be successfully applied to the important problem of constructing physical models. Indeed, this task consists of two steps: (i) choosing a basis with which to express the physical properties of interest and (ii) determining the coefficients associated with each basis function. Mathematically, the problem is completely analogous to the simple Fourier example considered above, with the sensing matrix  $\mathbf{A}$  being determined by the values of the basis functions at the chosen measurement points.

The conventional approach is to select a small, physically motivated basis set and to determine the unknown coefficients by performing a least-squares fit to the data.

While conceptually simple, this method is often difficult to use in practice. First, the number of unknown coefficients has to be smaller than the number of measurements, which precludes the use of very large basis sets. Second, finding the the optimal basis set is an  $NP$ -hard problem, i.e., the solution time increases faster than polynomial with the number of possible basis functions. Hence, the choice of the basis set has to be guided by physical intuition, which is hard to acquire and in many cases may not be available. Third, least-squares fitting is susceptible to noise, and there is often a possibility of “overfitting”—the model is trained to reproduce the fitting data, but performs poorly in a predictive capacity.

Compressive sensing offers a new paradigm for model building. Instead of attempting to develop physical intuition for which coefficients will be most relevant, the CS framework allows the inclusion of essentially all possible basis functions. Using very large basis sets eliminates the need to use physical intuition to construct smaller ones. Furthermore, CS is shown to be computationally efficient for very large problems, robust even for very noisy data, and produces more accurate models than current state-of-the-art approaches.

CS is applicable in any “sparse” basis-expansion problem, a broad class of problems in materials science. Among many possible choices that could be used for an example, we illustrate the power of the approach on a cluster expansion (CE) model because it is well-known and simple to understand. The CE method uses basis functions, defined over clusters of atomic sites, which describe the occupation of each site and thus the entire atomic configuration. The goal then is to determine which of the associated coefficients, of the thousands of possible choices, will contribute significantly to the property of interest. Physical intuition suggests that only a small number of them will be relevant, making CS applicable. For a more detailed description of the CE formalism see Appendix C.

## IV. APPLICATIONS

### A. Toy model example

We first work with an ad-hoc example where we choose a set of sparse coefficients and then use them to compute the energies of various crystal structures for use as input to CS. The advantage of this approach is that knowing the exact solution *a priori* allows us to easily determine the accuracy of the CS solution and determine how numerical noise influences the performance of the algorithm.

A total of 986 basis functions were used, and the coefficients of the three shortest nearest-neighbor pairs were chosen as 10, 4, and 1, respectively; all other coefficients were set to zero. Uniformly distributed random noise equal to  $\sim 10\%$ ,  $20\%$ , and  $50\%$  of the noiseless energies was added to the computed energies  $\tilde{f}$  to investigate the robustness of the CS formalism. In the presence of noise, the constraint of Eq. 2 may not be satisfied exactly, and we use the basis pursuit de-noising formulation given by Eq. (5) below. Here, one introduces a tunable parameter  $\mu$  that controls the sparsity of the resulting de-noised solution. We note that this algorithm recovers the exact solution to Eq. (3) in the noise-free case.

Figures 2(a) and 2(b) illustrate the performance of CS by showing two quantities: 1) the  $\ell_1$ -norm of the difference between the exact and fitted coefficients ( $\|J_{\text{exact}} - J_{\text{fit}}\|_1$ ), and 2) the number of non-zero coefficients ( $\ell_0$ -norm of the solution,  $\|J_{\text{fit}}\|_0$ ). We varied  $\mu$  to investigate its optimal values for a given noise level. Each data point in Fig. 2 was obtained by averaging over approximately 100 different sets, each of size  $N = 200$  or  $400$ .

The curves in Fig. 2 exhibit a series of plateaus, each one indicating a region over which the extracted solution remains practically unchanged. Notice, for example, the plateau located between  $\log_{10} \mu = -0.75$  and  $\log_{10} \mu = -0.4$  in the  $\|J_{\text{fit}}\|_0$  vs  $\mu$  curve for  $N = 200$  and the lowest noise content (circle markers). This plateau indicates that CS has extracted three non-zero coefficients. Furthermore, the value of  $\|J_{\text{exact}} - J_{\text{fit}}\|_1$  drops close to zero in this range, indicating that the CS has found essentially the exact answer. Using values of  $\mu$  below the optimal range results in sharp increases in both the number of nonzero coefficients and in the error  $\|J_{\text{exact}} - J_{\text{fit}}\|_1$ , indicating overfitting. Conversely,  $\mu$  values above the optimal range result in fewer non-zero coefficients and an incremental increase in  $\|J_{\text{exact}} - J_{\text{fit}}\|_1$ , indicating underfitting. As a function of increasing  $\mu$ , one first obtains a plateau where the CS reproduces the two largest expansion coefficients (10 and 4), followed by another plateau where only the largest coefficient is reproduced. This example illustrates the important point that CS is quite insensitive to the choice of  $\mu$ —the ability to recover the exact solution does not depend on the exact value of  $\mu$ , as long as it lies within an optimal (but broad) range.

Upon increasing the noise in the fitting data at a fixed data set size (compare the curves marked by circles and

squares in Fig. 2(a)), the plateaus in  $\|J_{\text{fit}}\|_0$  vs  $\mu$  become narrower until the highest plateau, corresponding to full recovery of the true solution, disappears completely (“x” markers in Fig. 2). At the same time, the minimum in the error  $\|J_{\text{exact}} - J_{\text{fit}}\|_1$  vs  $\mu$  is increasing incrementally. This displays the robustness and stability of CS, for even at a very high noise level we are able to recover the majority of the signal content.

Figure 2(c) displays  $\|J_{\text{exact}} - J_{\text{fit}}\|_1$ , averaged over approximately 100 random subsets, as a function of  $N$ , the number of fitting structures, and the noise level. Here we see the same plateau structure found in Fig. 2(a), with the lower (blue) plateau indicating essentially an exact fit. This plot demonstrates that, for all noise levels considered (up to as high as 50% of the noiseless energies), there remains a training set size for which the exact solution will be recovered.

### B. Actual alloy example: Ag-Pt

Having explained the basic properties of CS for a model system, we now test the performance of CS on real data for two very different systems: binary Ag-Pt alloys on a face-centered cubic (fcc) lattice and protein folding energies in the so-called zinc finger motif. Ag-Pt was chosen due to a report of unusual ordering tendencies<sup>17</sup> which are non-trivial to reproduce with current state-of-the-art CE methods, while the protein energetics represents a technically difficult test case with novel applications in biology.<sup>18,19</sup>

Out of the approximately 1100 crystal structures for which energies had been computed with quantum mechanics (see Appendix) in the Ag-Pt binary system, up to  $N = 400$  were chosen to be used as CS training data, and the rest were used for testing the predictive power of the energy model. We used a fixed  $\mu = 0.1$  for all training set sizes  $N$ , even though varying  $\mu$  with  $N$  could be advantageous; this is left for future studies as a possible refinement of the method. The  $\ell_0$ -norm of the solution and the root-mean-square (RMS) error over the prediction set were averaged over approximately 100 sets at each  $N$  as shown in Fig. 3.

To compare the performance of the  $\ell_1$ -based CS with other established methods, the state-of-the-art ATAT<sup>20</sup> software package, which employs a leave-one-out cross-validation (LOOCV) scheme, was applied to the same problem. Since a training set of size  $N = 400$  takes the LOOCV method several days to complete, averages were taken over only 10 training sets of size  $N$ . Fig. 3 shows the results of both the LOOCV and CS methods. In order to simulate building a complicated unknown model, we deliberately avoided applying physical intuition (e.g. picking short-range interactions) and simply performed the optimizations with minimal restrictions: using  $\mu = 0.1$  for CS and capping the maximum number of reported parameters to  $N/4$  for LOOCV to prevent excessive overfitting (see below). We see that CS achieves

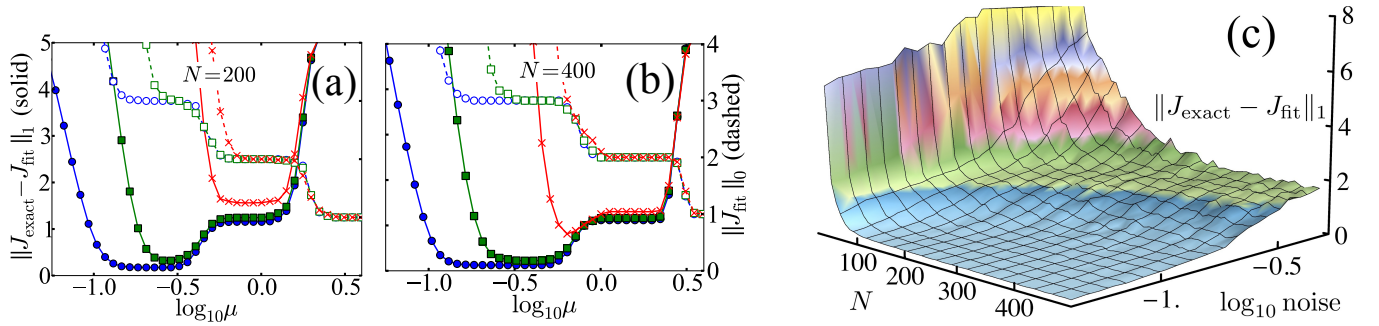


FIG. 2.  $\|J_{\text{exact}} - J_{\text{fit}}\|_1$  (solid) and  $\|J_{\text{fit}}\|_0$  (dashed) vs  $\log_{10}\mu$  for the toy model with  $N = 200$  (a) and  $N = 400$  (b). Random uniform noise of  $\sim 10\%$  (blue circles),  $20\%$  (green squares), and  $50\%$  (red “x”s) of the noiseless energies was added to the fitting structures. (c)  $\|J_{\text{exact}} - J_{\text{fit}}\|_1$  vs the number of fitting structures and the noise level. Each point represents an average over  $\sim 100$  different subsets of  $N$  structures.

an RMS error value much lower (6.5 meV/atom) than LOOCV (10.3 meV/atom). Furthermore, the number of non-zero coefficients found by LOOCV continuously increases with  $N$ , indicating overfitting, while the solution found by CS remains stable. This example shows that, in comparison with the traditional LOOCV-based method, CS is not only simpler and faster (less than a minute on a single CPU for CS *vs.* days for LOOCV at  $N = 400$ ), but also results in significant improvement in physical accuracy.

### C. Protein folding application

We now turn to a technically much more challenging case—that of protein design in biology. One of the key problems in protein design is to find the sequence of amino acids (AAs) which stabilizes a particular 3D structure, or *folding*. Physics-based energy functionals are considered to be some of the most-promising methods in protein design since they link the stability of the folded 3D structure to the total free energy, accurately accounting for electrostatics, van der Waals interactions, and solvation effects. However, their use is problematic due to the astronomical number of possible AA sequences for even very short proteins. It was shown<sup>18,19</sup> that the CE model can be generalized to describe protein energetics, allowing very fast direct evaluation of the protein energy as a function of its sequence.

Here, we use the data from Ref. 18 for the so-called zinc-finger protein fold. The fitting is done using a basis of approximately 76,000 clusters and energies of 60,000 AA sequences; a separate set of 4,000 AA sequence energies is used to test the predictive power of the CE model. The very large size of the problem presents a severe test to the conventional LOOCV-based model building approach, requiring running times of several weeks on parallel computers with user-supervised partial optimization.<sup>18</sup> We chose the highly efficient split Bregman iteration<sup>21</sup> for solving the basis pursuit denoising problem in Eq.(5), which allows us to perform a full opti-

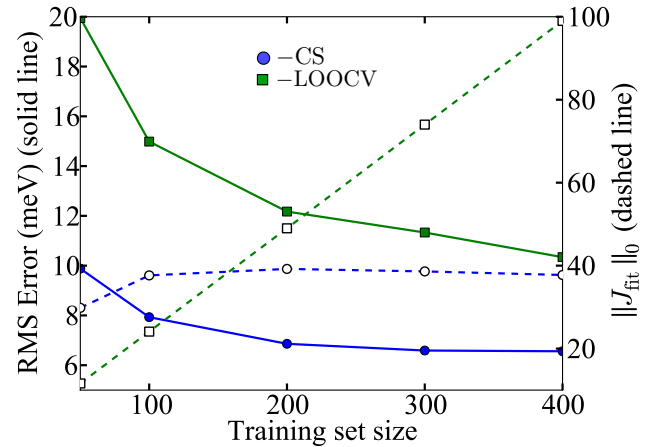


FIG. 3. Root-mean-square (RMS) errors for predictions (computed over all structures not used in the fit) and  $\ell_0$ -norm of the solution for the fcc Ag-Pt alloys vs. size of training set for compressive sensing (circles) and leave-one-out cross-validation scheme used by ATAT (squares).

mization in approximately 30 minutes on a single 2.4 GHz Intel Xeon E5620 processor. Figure 4 shows that for the physically important negative-energy configurations, we are able to achieve an RMS predictive error of 2.1 kcal/mol with 3,100 model parameters, significantly better than the RMS error of 2.7 kcal/mol with approximately 6,000 parameters obtained using the LOOCV method in Ref. 18. These results show that the computational efficiency, conceptual simplicity and physical accuracy of the  $\ell_1$ -based minimization has great potential for future applications in protein design.

## V. CONCLUSION

In conclusion, compressive sensing can be straightforwardly adopted to build physical models that are dominated by a relatively small number of contributions

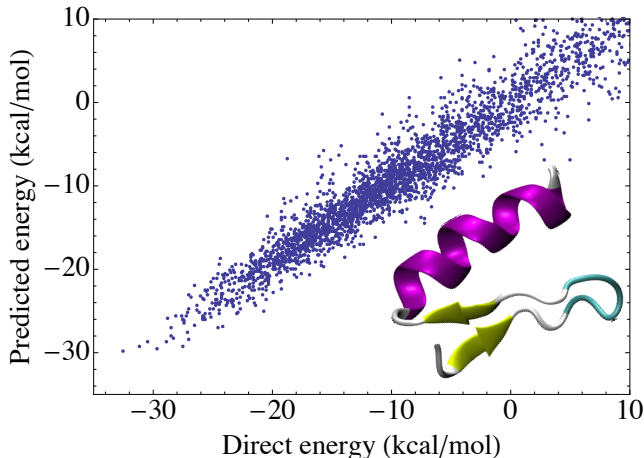


FIG. 4. Predictive performance of CS for protein energetics in the zinc-finger structure (shown in the inset).

drawn from a much larger underlying set of basis functions. Furthermore, many other scientific problems that do not appear to be a basis pursuit problem may be recast as one, in which case CS could efficiently provide accurate and robust solutions with relatively little user input. With the huge amount of experimental and computational data in physical sciences, compressive sensing techniques represent a promising avenue for model building on many fronts including structure maps, empirical potential models, tight binding methods, and cluster expansions for configurational energies, thermodynamics and kinetic Monte Carlo.

## ACKNOWLEDGMENTS

G. L. W. H. and L. J. N. are grateful for financial support from the NSF, DMR-0908753. F. Z. and V. O. were supported as part of "Molecularly Engineered Energy Materials," an Energy Frontier Research Center funded by the U.S. Department of Energy, Office of Science, Basic Energy Sciences under Award Number DE-SC0001342 and used computing resources at the National Energy Research Scientific Computing Center, which is supported by the US DOE under Contract No. DE-AC02-05CH11231.

## APPENDIX

### A. First-principles calculations

The energies of more than 1100 Ag-Pt fcc-based crystal structures were calculated from the density-functional theory (DFT) using the VASP software. We used projector-augmented-wave (PAW) potentials and exchange-correlation functionals parameterized by

Perdew, Burke and Ernzerhof under the generalized gradient approximation (GGA).<sup>22–24</sup> Equivalent  $k$ -points were used for Brillouin zone integration, to reduce systematic error.<sup>25</sup> Optimal choices of the unit cells, using a Minkowski reduction algorithm, were adopted to accelerate the convergence of the calculations. The effect of spin-orbit coupling was not included in our calculations for reasons fully explained in reference 26

Using the UNCLES<sup>27</sup> framework the following clusters on an fcc lattice were enumerated: 141 pairs, 293 triplets, 241 four-bodies, 87 five-bodies, and 222 six-bodies (986 clusters in total, including the onsite and empty clusters). The values of each of the 986 basis functions were computed for all structures in the fitting set, thus forming the sensing matrix,  $\mathbf{A}$ . In the ad hoc example with three nonzero interactions, the rows of the sensing matrix,  $\mathbf{A}$ , which each represent a fitting structure, were constructed by drawing randomly from a uniform distribution on  $[-1, 1]$ . For non-ad-hoc systems these rows should be mapped onto real crystallographic configurations. However since the quality of the fit was found to be unaffected by this mapping, either favorably or adversely, we chose to simply use the random vectors themselves in order to simplify computations. Real structures were used for Ag-Pt and protein cluster expansions.

### B. $\ell_1$ -based minimization

We adopt the definition of  $\ell_p$  norms:

$$\|u\|_p = \left( \sum_i |u_i|^p \right)^{1/p}, \quad (4)$$

of which the  $\ell_1$  (taxicab or Manhattan distance) and  $\ell_2$  (Euclidean; subscript 2 often omitted) norms are special cases. The number of non-zero elements of  $\vec{u}$  is often (improperly) referred to as the  $\ell_0$  "norm" even though it is not a norm in a strict mathematical sense.

The basis pursuit problem in Eq. (3) is a convex constrained minimization problem, which is somewhat difficult to solve due to the non-quadratic character of the objective function,<sup>28</sup> especially for large matrices  $\vec{A}$  when standard linear programming solvers perform poorly. In practice, it is often preferable to transform Eq. (3) into an unconstrained minimization problem:

$$\min_{\vec{u}} \mu \|\vec{u}\|_1 + \frac{1}{2} \|\mathbf{A}\vec{u} - \vec{f}\|^2, \quad (5)$$

This is especially advantageous when the data contains noise and the constraints given by Eq.(2) cannot be satisfied exactly; in the latter case, Eq. (5) is referred to as the basis pursuit denoising problem. Unfortunately, very small values of  $\mu$  are needed to recover the exact solution to the original basis pursuit problem in Eq. (3) without noise, which result in decreased efficiency of available numerical algorithms for solving Eq.(5). Yin *et al.*<sup>29</sup> proposed an efficient iterative algorithm for finding the solution to Eq. (5). Their method has the additional benefit

of yielding the exact solution to the original basis pursuit problem Eq. (3) for zero noise. This so-called Bregman iteration involves solving a small number (typically, 4 to 6) of problems of type Eq. (5) according to the following cycle ( $k = 0, 1, 2, \dots$ ):

$$\vec{f}^{k+1} = \vec{f} + (\vec{f}^k - \mathbb{A}\vec{u}^k), \quad (6)$$

$$\vec{u}^{k+1} = \arg \min_u \mu \|\vec{u}\|_1 + \frac{1}{2} \|\mathbb{A}\vec{u} - \vec{f}^{k+1}\|^2, \quad (7)$$

starting from  $\vec{f}^0 = \mathbf{0}$  and  $\vec{u}^0 = \mathbf{0}$ . The key feature of the algorithm is that the residual after iteration  $k$  is added back to the vector  $\vec{f}$  for the next iteration, resulting in efficient denoising and rapid convergence.<sup>29</sup> Each minimization in Eq. (7) was performed using the fixed-point continuation (FPC) method proposed by Hale, Yin, and Zhang.<sup>30</sup>

For the protein cluster expansion, the convergence rate of the FPC method was found to be very slow (presumably due to the size of the problem), and an improved algorithm due to Goldstein and Osher was found to be necessary.<sup>21</sup> This algorithm eliminates the hard-to-solve mixed  $\ell_1$  and  $\ell_2$  minimization problem in Eq. (7) by introducing a new variable  $\vec{d} = \mu\vec{u}$  and enforcing this equality by adding a new least-squares  $\ell_2$  term to the objective function:

$$\min_{u,d} \|\vec{d}\|_1 + \frac{1}{2} \|\mathbb{A}\vec{u} - \vec{f}\|^2 + \frac{\lambda}{2} \|\vec{d} - \mu\vec{u}\|^2. \quad (8)$$

The key advantage of this formulation is that the  $\ell_1$  minimization has to be performed with an  $\ell_2$  term that is diagonal in the components of  $d$ . The full split Bregman iterative algorithm proceeds as follows:

$$\vec{u}^{k+1} = \arg \min_u \frac{1}{2} \|\mathbb{A}\vec{u} - \vec{f}\|^2 + \frac{\lambda}{2} \|\vec{d}^k - \mu\vec{u} - \vec{b}^k\|^2, \quad (9)$$

$$\vec{d}^{k+1} = \arg \min_d \|\vec{d}\|_1 + \frac{\lambda}{2} \|\vec{d} - \mu\vec{u}^{k+1} - \vec{b}^k\|^2, \quad (10)$$

$$\vec{b}^{k+1} = \vec{b}^k + \mu\vec{u}^{k+1} - \vec{d}^{k+1}, \quad (11)$$

starting from  $\vec{d}^0 = \mathbf{0}$ ,  $\vec{b}^0 = \mathbf{0}$ , and  $\vec{u}^0 = \mathbf{0}$ . Eq. (9) now involves only  $\ell_2$  norms and can be solved efficiently using standard convex optimization, such as the conjugate gradient method.<sup>31</sup> The second step, Eq. (10), separates into individual vector components and can be easily solved in

one step as

$$d_n^{k+1} = \text{shrink}(\mu u_n^{k+1} + b_n^k, 1/\lambda), \quad (12)$$

where the shrinkage operator is defined as

$$\text{shrink}(y, \alpha) := \text{sign}(y) \max(|y| - \alpha, 0). \quad (13)$$

In other words, shrinkage decreases the absolute magnitude of  $y$  by  $\alpha$  and sets  $y$  to zero if  $|y| \leq \alpha$ .

### C. Cluster expansion

A useful model Hamiltonian for lattice configuration problems is the cluster expansion (CE).<sup>32–34</sup> The CE expresses the configurational dependence of a material's physical property as a sum over bonds. A particular configuration is given by a vector of atomic spins,  $\sigma$ , each component giving the occupancy corresponding to a different lattice site. The physical property of interest depends on the configuration,  $E(\sigma)$ , and can be decomposed into a sum over bonds. These bonds are often referred to as clusters in the cluster expansion community.

Mathematically, this idea is expressed as

$$E(\sigma) = \sum_F J_F \Pi_F(\sigma) \quad (14)$$

where  $\Pi_F$  is a product of atomic spin variables over cluster-class  $F$ , something commonly referred to as a correlation function. Each term in the expansion is a product between these correlation functions and an expansion coefficient  $J_F$ , also referred to as effective cluster interactions or ECIs. Since the correlation functions form a basis, the configurational dependence of any observable can be represented exactly by the cluster expansion if every term is retained. Since this is an impractical endeavor the expansion is typically truncated drastically, yielding an essentially equivalent expression for the observable. The CE can be used to quickly compute the energies of large numbers of configurations.

<sup>1</sup> A. Zunger, Phys. Rev. B **22**, 5839 (1980).

<sup>2</sup> P. Villars, Journal of the Less Common Metals **92**, 215 (1983).

<sup>3</sup> D. Pettifor, Solid State Communications **51**, 31 (1984).

<sup>4</sup> D. Pettifor, Journal of Physics C - Solid State Physics **19**, 285 (1986).

<sup>5</sup> A. Miedema, R. Boom, and F. R. De Boer, Journal of the Less Common Metals **41**, 283 (1975).

<sup>6</sup> C. C. Fischer, K. J. Tibbetts, D. Morgan, and G. Ceder, Nature Materials **5**, 641 (2006).

<sup>7</sup> J. C. Schön, K. Doll, and M. Jansen, physica status solidi

(b) **247**, 23 (2010).

<sup>8</sup> T. R. Munter, D. D. Landis, F. Abild-Pedersen, G. Jones, S. Wang, and T. Bligaard, Computational Science & Discovery **2**, 015006 (2009).

<sup>9</sup> W. Setyawan, R. M. Gaume, S. Lam, R. S. Feigelson, and S. Curtarolo, ACS Combinatorial Science **13**, 382 (2011), <http://pubs.acs.org/doi/pdf/10.1021/co200012w>.

<sup>10</sup> S. M. Woodley and R. Catlow, Nature Materials **7**, 937 (2008).

<sup>11</sup> A. P. J. Jansen and C. Popa, Phys. Rev. B **78**, 085404 (2008).

- <sup>12</sup> T. Müller and G. Ceder, Phys. Rev. B **80**, 024103 (2009).
- <sup>13</sup> E. Cockayne and A. Van De Walle, Phys. Rev. B **81**, 012104 (2010).
- <sup>14</sup> E. Candès and M. Wakin, Signal Processing Magazine, IEEE **25**, 21 (2008).
- <sup>15</sup> M. AlQuraishi and H. McAdams, Proceedings of the National Academy of Sciences **108**, 14819 (2011).
- <sup>16</sup> E. Candès, J. Romberg, and T. Tao, Information Theory, IEEE Transactions on **52**, 489 (2006).
- <sup>17</sup> P. Durussel and P. Feschotte, J. Alloys Compound. **239**, 226 (1996).
- <sup>18</sup> F. Zhou, G. Grigoryan, S. Lustig, A. Keating, G. Ceder, and D. Morgan, Physical review letters **95**, 148103 (2005).
- <sup>19</sup> G. Grigoryan, A. Reinke, and A. Keating, Nature **458**, 859 (2009).
- <sup>20</sup> A. Van de Walle, M. Asta, and G. Ceder, Calphad **26**, 539 (2002).
- <sup>21</sup> T. Goldstein and S. Osher, SIAM Journal on Imaging Sciences **2**, 323 (2009).
- <sup>22</sup> G. Kresse and D. Joubert, Phys. Rev. B **59**, 1758 (1999).
- <sup>23</sup> G. Kresse and J. Furthmüller, Comp. Mat. Sci. **6**, 15 (1996).
- <sup>24</sup> P. E. Blöchl, Phys. Rev. B **50**, 17953 (1994).
- <sup>25</sup> S. Froyen, Phys. Rev. B **39**, 3168 (1989).
- <sup>26</sup> L. Nelson, G. Hart, and S. Curtarolo, Phys. Rev. B **85**, 054203 (2012).
- <sup>27</sup> D. Lerch, O. Wieckhorst, G. L. W. Hart, R. W. Forcade, and S. Müller, Modelling and Simulation in Materials Science and Engineering **17**, 055003 (2009).
- <sup>28</sup> S. Chen, D. Donoho, and M. Saunders, Siam Review **43**, 129 (2001).
- <sup>29</sup> W. Yin, S. Osher, D. Goldfarb, and J. Darbon, SIAM Journal on Imaging Sciences **1**, 143 (2008).
- <sup>30</sup> E. Hale, W. Yin, and Y. Zhang, CAAM TR07-07, Rice University (2007).
- <sup>31</sup> S. Boyd and L. Vandenberghe, *Convex Optimization* (Cambridge University Press, 2004).
- <sup>32</sup> J. Sanchez, F. Ducastelle, and D. Gratias, Physica A: Statistical and Theoretical Physics **128**, 334 (1984).
- <sup>33</sup> D. Fontaine, Solid State Physics **47**, 33 (1994).
- <sup>34</sup> A. Zunger, “First-principles statistical mechanics of semiconductor alloys and intermetallic compounds,” (NATO Advanced Study Institute on Statics and Dynamics of Alloy Phase Transformations, 1994) pp. 361–419.